lncRNA MIR17HG Directs Cooperative Epigenetic Regulation in Colorectal Cancer

Jie Xu[1, #], Qingtao Meng[1, #], Xiaobo Li[1], Hongbao Yang[2], Jin Xu[3], Na Gao[1], Hao Sun[1], Shenshen Wu[1], Giuseppe Familiari[4], Michela Relucenti[5], Haitao Zhu[6], Jiong Wu[7], Rui Chen[1,8 *]

[1]Key Laboratory of Environmental Medicine Engineering, Ministry of Education, School of Public Health, Southeast University, Nanjing 210009, China

[2]Center for New Drug Safety Evaluation and Research, China Pharmaceutical University, Nanjing 211198, China

[3]Department of Maternal, Child and Adolescent Health, School of Public Health, Nanjing Medical University, Nanjing 211166, China

[4]Department of Anatomical, Histological, Medical and Legal locomotive Apparatus, Section of Human Anatomy Via Alfonso Borelli, Sapienza University of Rome, Roma 5000161, Italia

[5]Department of Anatomical, Histological, Forensic Medicine and Orthopedic Science, Sapienza University of Rome, Roma 5000161, Italia

[6]Colorectal Cancer Center, Department of General Surgery, Jiangsu Cancer Hospital, Cancer Research Institute, Cancer hospital of Nanjing Medical University, Nanjing 210009, China

[7] School of Life Sciences, Jiangsu Normal University, Xuzhou, 221116, China

[8]Institute for Chemical Carcinogenesis, Guangzhou Medical University, Guangzhou 511436, China

Running title: MIR17HG epigenetic regulation in colorectal cancer

Key words: long non-coding RNA; MIR17HG; colorectal cancer; NF-κB/RELA; WGCNA

[#] These two authors contribute equally

[*]**Correspondence author: Rui Chen**, Key Laboratory of Environmental Medicine Engineering, Ministry of Education, School of Public Health, Southeast University, 87 Dingjiaqiao, Gulou District, Nanjing 210009, China. Tel: +86 25 83272560; Fax: +86 25 83324322; Email: 101011816@seu.edu.cn.

Disclosure of Potential Conflicts of Interests：

The authors declare no conflict of interest.

Abstract

Immune dysregulation plays a vital role in colorectal cancer (CRC) initiation and progression. Long non-coding RNA (lncRNA) exhibits multiple functions including the epigenetic control of gene expression. Here, we identified an immune-related lncRNA, MIR17HG, whose expression was gradually upregulated in adjacent, adenoma and CRC tissue. MIR17HG promoted tumorigenesis and metastasis in CRC cells both in vitro and in vivo. Mechanistically, MIR17HG increased the expression of nuclear factor kappa B(NF-κB)/RELA by competitively sponging the microRNA miR-375. In addition, RELA transcriptionally activated MIR17HG in a positive feedback loop by directly binding to its promoter region. Moreover, miR-17-5p, one of the transcribed miRNAs from MIR17HG, reduced the expression of the tumor suppressor B Cell Linker (BLNK) resulting in increased migration and invasion of CRC cells. MIR17HG also upregulated PD-L1, indicating its potential role in immunotherapy. Overall, these findings demonstrate that MIR17HG plays an oncogenic role in CRC and may serve as a promising therapeutic target.

Significance

Findings provide mechanistic insight into the role of the long non-coding RNA MIR17HG and its miRNA members in regulating colorectal cancer carcinogenesis and progression.

Introduction

Colorectal cancer (CRC) is a severe health threat worldwide (1). Although remarkable progress has been made in the past decades, the molecular mechanisms underlying CRC carcinogenesis and progression remain unclear. Thus, novel biomarkers for early screening and therapeutic intervention are urgently demanded. In previous studies, the association between chronic inflammation and CRC has been extensively exploited (2). Nuclear factor kappa B (NF-κB) is a master regulator of inflammation and inflammation-associated cancer (3). NF-κB promotes the secretion of pro-inflammatory cytokines and regulates the cell cycle and survival of CRC cells (4, 5). Given its importance, NF-κB and its upstream and downstream networks present potential targets for therapeutic interventions.

Long non-coding RNAs (lncRNAs) are a class of transcripts longer than 200 nucleotides with little protein-coding capacity (6). Massive evidence suggests that lncRNAs are implicated in various biological processes of cancer, including differentiation, proliferation, apoptosis, metastasis, and drug-resistance (6-8). Although several lncRNAs and their underlying mechanisms in CRC have been reported previously (9, 10), the cross-talk between NF-κB, lncRNAs and mRNAs in CRC progression remains unknown.

Genomic approaches involving mRNA, microRNA (miRNA), or lncRNA microarrays coupled with scale-free network analyses have been applied to explore the mechanisms of cancer initiation and progression (11, 12). Weighted gene co-expression network analysis (WGCNA) facilitates the identification of core gene networks based on similar gene expression patterns across samples (13). The clustered cores or modules identified by WGCNA often represent genes involved in particular

biological functions that are either co-expressed or co-regulated according to cell type or biological condition (14).

In this study, we used WGCNA to profile differentially expressed lncRNAs and mRNAs in adjacent, adenoma, and CRC tissues and constructed an lncRNA–transcription factor (TF)–mRNA network. The lncRNA MIR17HG stood out as a key modulator in a feedback loop with NF-κB. Moreover, MIR17HG coordinated with miR-17-5p, thereby negatively regulating BLNK expression. In addition, MIR17HG directly bound and upregulated PD-L1, indicating its potential role in immunotherapy. These findings indicated an oncogenic role for MIR17HG in CRC and elucidated its significance in immunotherapy.

Materials and Methods

The complete details of all reagents and procedures used in this study are provided in the SI Appendix and SI Materials and Methods.

Patients and specimens

All the participants signed written informed consent form before recruitment. The study was conducted in accordance with Declaration of Helsinki and approved by the Ethics Committee of Southeast University Affiliated Zhongda Hospital.

The tissue samples used for microarray analysis were obtained from 6 CRC patients and 6 adenoma patients. Detailed clinical information is shown in Supplementary Table 1.

CRC and matched adjacent tissues (5 cm from the tumor margin) from 2 independent cohorts were used for tissue microarray (TMA) construction. Two independent cohorts were enrolled in this study between January 2007 and October 2011. In the testing cohort, 376 CRC patients were enrolled at the Affiliated Hospital of Xuzhou Medical University. In the validation cohort, 431 CRC patients were enrolled at the Jiangsu Tumor Hospital. All patients were newly-diagnosed and histologically-confirmed CRC cases with no preoperative chemo/radiotherapy. Detailed information is presented in Supplementary Table 2. Signed informed consent was provided by each subject before recruitment. The pathological stage of CRC was assessed by the 6th edition of the American Joint Committee on Cancer (AJCC) cancer

staging manual. All patients were followed up in person or by phone until the time of death or last follow-up (June 2016). The maximum follow-up time was 112.7 months with a median survival time (MST) of 67.1 months.

Fresh CRC and the corresponding adjacent tissues as well as colorectal adenoma (ADE) tissues were collected at the Jiangsu Tumor Hospital and the Affiliated Hospital of Xuzhou Medical University from 2014 to 2015. Detailed information is presented in Supplementary Tables 3 and 4. The expression levels of the indicated lncRNAs, miRNA and mRNA were detected in these tissues.

Weighted gene co-expression network analysis (WGCNA)

A co-expression network for lncRNAs and mRNAs was built using the WGCNA package in R (13). WGCNA provides information about each gene, summary statistics, and module membership (i.e., a measure of how strongly the expression profile of a gene correlates with that of the module) that can be used to screen candidate genes for further functional studies. To construct a scale-free network, Pearson's correlation matrix was determined for all gene pairs and transformed into an adjacency matrix using the power function. Next, a weighted network was created. Module is defined as a group of densely interconnected molecules with high topological overlap in the weighted network analysis.

Cell lines and transfection

The cell lines HCT15, HCT116, SW480, SW620, HT29, DLD-1, RKO and LoVo were obtained from American Type Culture Collection (ATCC) in 2016. These cells

were tested by short tandem repeat analysis, validated to be free of mycoplasma, which were used within 6 months. In addition, the cells were cultured within 25 passages for all experiments. All cell lines were maintained in Dulbecco's Modified Eagle's Medium (DMEM; Gibco, USA), 10 % (v/v) fetal bovine serum (FBS; Sigma, USA), 100 U/mL penicillin (Gibco), and 100 μg/mL streptomycin (Gibco) at 37 °C in 5% CO_2.

Transfection was performed with Lipofectamine 2000 (Invitrogen, USA) or Lipofectamine RNAiMAX (Invitrogen) according to the manufacturer's protocols. The small interfering RNA (siRNA) of MIR17HG silencer RELA was purchased from Guangzhou RiboBio Co. Ltd, China.

Tissue microarray (TMA)

Paraffin-embedded blocks of cancer tissue and matched adjacent tissue specimens from the testing and validation cohorts were used for TMA construction at the National Engineering Center for Biochip (Shanghai, China). For each case, 1 mm cores were transferred to a TMA block. The biopsies of adjacent colorectal epithelial tissues were then inserted into the center of each slide with the 4 angles used as negative controls.

Chromatin immunoprecipitation (ChIP) assay

ChIP assay was performed with the EZ-ChIP Chromatin Immunoprecipitation Kit (Millipore, USA). Briefly, cross-linked chromatin DNA was proceeded by sonication into 200-500 base pair (bp) fragments. Then, chromatin was

immunoprecipitated with the corresponding antibodies. The isolated DNA was assessed by quantitative real-time PCR (qRT-PCR) using SYBR Green Mix (Takara, Japan).

RNA immunoprecipitation (RIP) assay

The SW620 cells were co-transfected with MS2 plasmids (Genaray, China). After 48 h, the cells were subjected to RIP assay using the Magna RIP RNA-Binding Protein Immunoprecipitation Kit (Millipore) according to the manufacturer's instructions. The abundance levels of co-precipitated RNAs were detected by qRT-PCR. Total RNA (input controls) and the IgG controls of the corresponding species were assayed simultaneously.

Animals

Mice were housed (5 animals per cage) on corncob bedding with food and water ad libitum, and they were handled according to the guidelines of the Committee on Animal Use and Care of Southeast University.

RELA$^{-/-}$ mouse establishment

In this study, RELA^{fl} (B6.129S1-*Rela*^{tm1Ukl}/J, Stock No: 024342) mice were purchased from the Jackson Laboratory (Bar Harbor, ME USA). PVillin-Cre mice (B6/JNju-Tg(PVillin-Cre)D/Nju), which express Cre recombinase specifically in the intestine, were purchased from Model Animal Research Center of Nanjing University,

China. To generate the $RELA^{-/-}$ mice, $RELA^{fl/fl}$ mated with PVillin-Cre transgenic mice to obtain $RELA^{+/-}$ mice. Next, we caged $RELA^{fl/fl}$ and $RELA^{+/-}$ mice to obtain $RELA^{Flox/Flox}$; PVillin-Cre mice which we called $RELA^{-/-}$ mice here since we only had one type of conditional KO mice in this study.

$RELA^{fl/fl}$ and $RELA^{-/-}$ mice (30 mice per group) were intraperitoneally injected with 10 mg/kg azoxymethane (AOM) (Sigma). One week later (Day 7), all mice were administered 2.5% (w/v) dextran sulfate sodium (DSS) (MW: 36, 000–50, 000, ICN Pharmaceuticals, USA) in drinking water for 3 cycles of 5 days of DSS and 16 days of regular drinking water. Mouse death was monitored. A total of 10 mice per group were sacrificed on Day 84 (14 days after the end of the third DSS treatment cycle), then colorectal tumor formation was observed. After sacrifice, 6 of the 10 colon tissues were fixed with 4% paraformaldehyde (PFA), and the remaining 4 were snap frozen in liquid nitrogen. The remaining mice were maintained until Day 120. A combined pathological score ranging from 0 to 6 was used to evaluate DSS-induced colitis (6).

Xenograft assays in vivo

Female nude mice (18-20 g) were purchased from Model Animal Research Center of Nanjing University, China. Nude mice were injected subcutaneously on the dorsal flank with 5×10^6 luciferase-expressing, stably-transformed cells suspended in 0.2 mL DMEM. Three weeks after injection, the mice were sacrificed under ether

anesthesia. Lung, liver, and xenograft tissues were removed, and luciferase activities were determined on a luminometer (Sirius, Berthold Detection Systems, Germany).

Statistical analysis

The $\chi 2$-test was used to evaluate the associations of MIR17HG expression with clinical variables. The Wilcoxon test was used to assess the differences in MIR17HG, BLNK and RELA staining scores in the TMA. Log-rank test was used to analyze the survival curves. Fisher r-to-z transformation test followed by the Pearson correlation test was used to analysis the correlation. Hazard ratios (HRs) and 95%CIs were determined by univariate or multivariate Cox regression analysis with adjustments for age, gender, location (colon or rectum), grade (low or intermediate/high differentiation), and clinical stage (I/II or III/IV). Statistical analysis was performed with SPSS 21.0 with $P < 0.05$ considered statistically significant.

Results

Construction of a lncRNA and mRNA network involved in CRC progression by WGCNA systemic analysis

The lncRNA and mRNA expression profiles of CRC, colorectal adenoma and adjacent tissues (n = 6 in each condition) were determined by microarray analysis (Fig. 1A, B). To further assess lncRNA and mRNA co-expression patterns, WGCNA was used to identify genes that played pivotal roles in CRC development. A total of 27 modules were identified (Fig. 1C), including 10 that were significantly correlated with CRC progression. In contrast, these modules showed no clear associations with gender, and only some of them were associated with age (Fig. 1D). Wilcoxon test results revealed that Module 1 (M1), Module 14 (M14), and Module 15 (M15) were gradually increased or decreased from adjacent, colorectal adenoma to CRC tissue samples, with no effects of age and gender observed in the 27 modules (Fig. 1E). Thus, we focused on M1, M14, and M15 in subsequent experiments.

Based upon microarray profiles in these three modules, the heat map (Supplementary Fig. S1A) and differentially expressed genes (DEGs) in the modules were analyzed using the Kyoto Encyclopedia of Genes and Genomes (KEGG) database to identify the corresponding biological pathways (Supplementary Fig. S1B). DEGs in both M1 and M14 showed significantly enriched KEGG pathways ($P < 0.05$), including immunity-associated pathways; however, there was no markedly enriched

KEGG pathways in M15. Therefore, the emerged mRNAs in M1 and M14 were pooled for sequential analysis, revealing an integrated network of mRNAs and their correlated lncRNAs (fold change (FC) > 1.5) that were involved in immunity-associated pathways (Fig. 1F). Traditionally, the mechanism of competing endogenous RNAs (ceRNAs) is employed to explore the detailed connections between the targeted lncRNAs and mRNAs. In this study, the complex network was assessed at the transcriptional level. Thus, to further explore key connection nodes in immunity pathways between M1 and M14, we initially constructed a gene-TF regulatory network for M14 in which a subunit of NF-κB, RELA, was identified as the transcription factor with the highest degree (Fig. 1G). Subsequently, bioinformatics analysis suggested that NF-κB, a traditional transcription factor in the immune response, was also transcriptionally related to the M1 immune pathway–involved genes. It turned out that NF-κB transcriptionally regulated 19 mRNAs and was associated with 21 lncRNAs involved in the M1 immune pathway (Fig. 1H). These findings suggested that the cross-talk between immune pathways in M1 and M14 was linked by NF-κB, including a total of 9 lncRNAs and 19 mRNAs (Fig. 1I).

MIR17HG is upregulated in CRC and transcriptionally activated by NF-κB/RELA

The expression patterns of the 9 lncRNAs involved (Fig. 1I) were validated by qRT-PCR in fresh tumor, adenoma, and adjacent tissues (n = 96 per group). The

results showed increasing expression patterns for MIR17HG and LINC00460, with gradually decreasing expression levels of XLOC_006495, from adjacent to adenoma, and CRC tissues (Fig. 2A, left panel and Supplementary Fig. S1C). Moreover, the expression levels of RELA, the key connection node between M1 and M14, were gradually accumulated from adjacent to adenoma, and CRC tissues (Fig. 2A, right panel), which is consistent with the data retrieved from the Cancer Genome Atlas (TCGA) (Supplementary Fig. S1D). Finally, according to the above experimental data, the co-expression network constructed in Fig. 1I was reorganized as illustrated in Supplementary Fig. S1E.

To further define the associations of the 3 lncRNA candidates with RELA, knockdown assays were performed using siRNAs. As shown in Fig. 2B, MIR17HG levels were significantly blunted after RELA knockdown in all tested CRC cell lines. Correspondingly, RELA was also attenuated after MIR17HG ablation in 8 CRC cell lines. However, this correlational regulation did not occur for LINC00460 and XLOC_006495 (Supplementary Fig. S1F).

Given the importance of RELA in the TF regulatory network, we assessed the role of RELA in CRC progression using mice models. $RELA^{fl/fl}$ and $RELA^{-/-}$ mice were studied using an azoxymethane-dextran sodium sulfate (AOM-DSS) model. As illustrated in Fig. 2C, colon shortening, which is the macroscopic parameter of colitis severity, was more pronounced in AOM-DSS–treated $RELA^{fl/fl}$ mice compared with

RELA$^{-/-}$ mice (4.585±0.549 cm vs. 5.917±0.728 cm). Both RELA$^{fl/fl}$ and RELA$^{-/-}$ mice developed tumors in the middle and distal colons; however, RELA$^{fl/fl}$ mice developed a markedly greater number of tumors, higher tumor formation rate, and shorter overall survival time (Fig. 2C, right panel and Fig. 2D). Histological examination consistently showed low- to medium-grade neoplasia in RELA$^{-/-}$ mice compared to medium- to high-grade in RELA$^{fl/fl}$ mice (Supplementary Fig. S2A). Similarly, RELA levels displayed an increasing trend from adjacent to adenoma, and CRC tissues in RELA$^{fl/fl}$ mice, but not in RELA$^{-/-}$ mice (Fig. 2E).

To seek the sequential events involved in the RELA-related CRC carcinogenesis, MIR17HG expression levels were detected in RELA$^{fl/fl}$ compared with RELA$^{-/-}$ mice in the AOM-DSS model. *In situ* hybridization (ISH) demonstrated that MIR17HG exhibited an increasing trend from adjacent to adenoma, and CRC tissues in RELA$^{fl/fl}$ mice, but not in RELA$^{-/-}$ mice (Fig. 2F). Collectively, these results suggested that RELA transcriptionally regulated MIR17HG in murine colorectal tumorigenesis. In using ChIP assays to further assess the biological relationship between MIR17HG and RELA, the RELA protein was found to directly bind to the specific motif in the MIR17HG promoter region (Fig. 2G).

In addition, the MIR17HG expression pattern positively correlated with the RELA mRNA levels in CRC patients (n = 96) (Supplementary Fig. S2B). Furthermore, based upon the ISH analysis from tissue microarray (TMA) with five years survival

information, the data showed that the relative expression levels of MIR17HG and RELA were dramatically accumulated in CRC tumor tissues compared with adjacent tissues not only in the testing but also in the validation cohorts (Fig. 2H and Supplementary Fig. S2C). Moreover, Kaplan-Meier (KM) analysis showed that patients with high expression of both RELA and MIR17HG gained a significantly shorter overall survival time than those with low levels (Fig. 2I and Supplementary Fig. S2D). Taken together, these findings indicated that MIR17HG was transcriptionally activated by NF-κB/RELA. Therefore, further assessment of the MIR17HG function in CRC was important.

MIR17HG promotes CRC growth and metastasis through suppressing BLNK expression binding with miR-17-5p

Typically, MIR17HG is the miR-17-92 cluster host gene, which has been reported to promote carcinogenesis in different tumors (15, 16). BLNK, previously identified in the network of M14, was predicted to be targeted by the miR-17-92 cluster in the miRBase and TargetScan database (Fig. 3A). Data retrieved from TCGA showed significantly higher expression levels of the miR-17-92 cluster (miR-17-5p, miR-17-3p and miR-19b-1-5p) in CRC tissues compared with normal ones (Supplementary Fig. S3A). Only miR-17-5p was differentially expressed among adjacent, adenoma, and CRC tissue samples among these three miRNAs as quantified using qRT-PCR (Fig. 3B, left panel). Subsequently, the role of miR-17-5p in the

tumorigenesis of CRC was explored. SW620 and HCT116 cells lost colony formation, migration, and invasion capabilities, as well as tumor formation and metastasis lacking the miR-17-5p (Supplementary Fig. S3B-E). As shown in Supplementary Fig. S3F, G, miR-17-5p augmentation in CRC tumor compared with adjacent tissues by TMA and KM analysis. Clearly, the mean overall survival time in patients with relatively high miR-17-5p expression was decreased significantly in the testing and/or validation cohorts. Moreover, as the predicted target gene for the miR-17-92 cluster, BLNK displayed a reverse trend compared with miR-17-5p in tissues (Fig. 3B, right panel). Consistently, data retrieved from TCGA suggested significantly lower expression levels of BLNK in CRC compared with that of normal tissues (Supplementary Fig. S4A).

To verify BLNK regulation by miR-17-5p, luciferase reporter assays were performed in SW620 and HCT116 cells. The overexpression of miR-17-5p resulted in the blunting of the luciferase activity of wild type but not the mutated BLNK 3′UTR, which suggested that miR-17-5p directly regulated BLNK expression by binding the BLNK 3′UTR (Fig. 3C). We then tested if MIR17HG regulated BLNK through miR-17-5p. Our data showed that the mRNA levels of BLNK were increased by miR-17-5p or MIR17HG individual knockdown and blunted with either miR-17-5p or MIR17HG overexpression (Supplementary Fig. S4B). Furthermore, the co-overexpression of MIR17HG and miR-17-5p decreased BLNK expression, and the double knockdown of MIR17HG and miR-17-5p showed the opposite effect (Fig. 3D).

Notably, BLNK was upregulated after MIR17HG overexpression while miR-17-5p was knocked down. In contrast, BLNK was decreased after MIR17HG knockdown combined with miR-17-5p overexpression (Fig. 3E), which suggested that MIR17HG might be an upstream regulator of miR-17-5p and BLNK. In addition, miR-17-5p expression was negatively correlated to BLNK mRNA levels in CRC, which was similar to the relationship between MIR17HG and BLNK (n = 96) (Supplementary Fig. S4C). Accordingly, we confirmed the MIR17HG/miR-17-5p/BLNK molecular cascade in colorectal cells (Fig. 3F).

The suppression of BLNK has been reported in different tumor tissues (17-19); however, the role of BLNK in CRC tumorigenesis remains unclear. Here, SW620 and HCT116 cells were stably transfected with BLNK shRNA and a non-targeting shRNA control labeled with firefly luciferase. Blunt of BLNK strikingly accumulated colony formation, migration, and invasion abilities in both SW620 and HCT116 cells (Fig. 3G and Supplementary Fig. S4D). In agreement, *in vivo* data showed that increased tumor volumes were observed in nude mice lacking BLNK. The same pattern was observed with liver and lung luciferase biochemical measurements, with markedly promoted liver and lung metastasis in mice carrying flank tumors expressing low levels of BLNK (Fig. 3H and Supplementary Fig. S4E). Moreover, TMA analysis showed that BLNK expression levels were reduced dramatically in CRC tumor tissues compared with adjacent samples (Fig. 3I and Supplementary Fig. S4F). Consistently, KM analysis revealed that the mean overall survival time was significantly decreased

in patients with relatively low BLNK expression (Fig. 3J and Supplementary Fig. S4G).

RELA attenuates BLNK expression through activating MIR17HG

Given that MIR17HG and the miR-17-92 cluster are transcribed from the same locus, and that MIR17HG was transcriptionally upregulated by RELA, we evaluated whether RELA could transcriptionally activate the miR-17-92 cluster. Therefore, we detected miR-17-3p, miR-19b-1-5p, and miR-17-5p expression levels in $RELA^{fl/fl}$ and $RELA^{-/-}$ mice by ISH assay. The results showed that only miR-17-5p was blunted in colorectal adenoma and cancer tissues from $RELA^{-/-}$ mice, but not in the $RELA^{fl/fl}$ mice (Fig. 4A and Supplementary Fig. S5A and B).

Based upon the previous findings on the two regulatory cascades of MIR17HG/miR-17-5p/BLNK and RELA/miR-17-5p in the CRC carcinogenesis, we next assessed if BLNK was directly regulated by RELA. Interestingly, compared with the miR-17-5p results, the opposite was observed for BLNK as protein levels were instead gradually reduced from adjacent to adenoma, and CRC tissues in $RELA^{fl/fl}$ mice, with no differences identified due to the lack of RELA (Fig. 4B). Furthermore, we confirmed the specific regulation pattern of BLNK by RELA in CRC cell lines. Both the BLNK augmentation of RELA knockdown and BLNK attenuation of RELA overexpression were clearly observed (Fig. 4C). Additionally, the *in vitro* modulation of BLNK expression by RELA indicated that the latter was upstream of MIR17HG in

the molecular cascade (Fig. 4D, E). Taken together, these data revealed the molecular pathway of RELA/MIR17HG/miR-17-5p/BLNK in CRC tumorigenesis (Fig. 4F).

To further clarify these molecular pathway events of MIR17HG, RELA, miR-17-5p and BLNK on the clinicopathological characteristics of CRC patients, multivariate regression analysis was performed in the testing and/or validation cohorts. As shown in Table 1, high expression levels of MIR17HG, RELA and miR-17-5p, advanced tumor stage, and advanced age were associated with shorter survival in all cohorts. Meanwhile, BLNK expression appeared to be a positive prognostic factor in CRC patients. Considering that the expression patterns of MIR17HG and miR-17-5p displayed a strong consistency, we reassessed the correlation between their expression levels in combination and prognosis in CRC patients. The results suggested that survival time in patients with a high expression of either MIR17HG or miR-17-5p was between those of patients with MIR17HG plus miR-17-5p at high levels and the ones expressing low amounts of MIR17HG plus miR-17-5p (Supplementary Fig. S5C).

MIR17HG accumulates RELA expression by sponging miR-375

lncRNAs work as ceRNAs by competitively sponging miRNAs, resulting in the liberation of target mRNAs (20-22). Because WGCNA analysis indicated that MIR17HG potentially activated RELA in M1, we hypothesized that MIR17HG regulated RELA MALT1, NFKBIE, PPP3R1, MAP3K7, and CBL through sponging miRNAs which blunt them on the 3′UTR. Indeed, two miRNAs, miR-375 and miR-2116-5p, were predicted to be sponged by MIR17HG via miRBase and

TargetScan database analyses (Fig. 5A). To determine if MIR17HG bound to the endogenous miR-375/miR-2116-5p, MS2-based RIP assays were performed. The results showed that MIR17HG was markedly enriched for miR-375 compared with miR-2116-5p, but not the MIR17HG with mutated miR-375 targeting sites (Fig. 5B). Interestingly, the expression levels of miR-375 in human adjacent, adenoma, and tumor tissues were not significantly altered (Fig. 5C), which means that miR-375 only served as a scaffold to connect MIR17HG and activated mRNAs.

As a proof-of-concept, the luciferase reporter assay was performed firstly to confirm RELA, MALT1, NFKBIE, PPP3R1, MAP3K7, and CBL regulation by miR-375. Except for CBL, luciferase activities were attenuated after cell co-transfection with miR-375 and wild types of RELA, MALT1, NFKBIE, PPP3R1 and MAP3K7 3′UTR, but not the mutant variants, indicating that miR-375 directly targeted these 5 genes (Fig. 5D and Supplementary Fig. S6A). Furthermore, the expression levels of MALT1, NFKBIE, PPP3R1, MAP3K7, and RELA all displayed a significant trend of increasing expression from adjacent to adenoma, and CRC tissues, corroborating the data retrieved from TCGA (Fig. 2A and Supplementary Fig. S1D, S6B). Moreover, correlation analysis showed that MIR17HG was significantly associated with RELA, MALT1, NFKBIE, PPP3R1, and MAP3K7 mRNA levels in CRC (Supplementary Fig. S2B and S6B). These findings suggested that MIR17HG activated RELA, MALT1, NFKBIE, PPP3R1, and MAP3K7 in CRC through ceRNA mechanism on miR-375.

MIR17HG plays an oncogenic role in CRC tumorigenesis through building a positive feedback loop with RELA

Since RELA was involved in this regulatory network of ceRNAs, we further assessed RELA regulation by MIR17HG with or without miR-375. The results showed that RELA expression levels were elevated after MIR17HG overexpression (Fig. 5E, left panel). Consistently, results were observed after MIR17HG overexpression + miR-375 suppression in cells (Fig. 5E, right panel). Notably, compared with MIR17HG overexpression + miR-375 negative control, the expression level of RELA with MIR17HG overexpression + miR-375 overexpression was significantly inhibited in HCT116 and SW620 cells (Fig. 5F), suggesting the ability of MIR17HG to sponge miR-375 regulate expression of RELA. As previously demonstrated, RELA transcriptionally regulated MIR17HG expression (Fig. 2G). Combined with the current findings, these results indicated a positive feedback loop between MIR17HG and RELA in CRC tumorigenesis (Fig. 5G).

Taken together, MIR17HG not only inhibited BLNK expression through its cluster member miR-17-5p in CRC, but also formed a positive feedback loop with RELA. Accordingly, we further assessed the role of MIR17HG in CRC tumorigenesis. As shown in Fig. 2A, MIR17HG was upregulated in CRC compared with adjacent and adenoma tissues. To evaluate the oncogenic properties of MIR17HG in CRC, SW620 and HCT116 cells were transfected with MIR17HG shRNA and a non-targeting shRNA control labeled with firefly luciferase. *In vitro* assays indicated

that MIR17HG knockdown in SW620 and HCT116 cells resulted in significantly decreased colony formation, migration, and invasion abilities (Fig. 5H, I). MIR17HG knockdown markedly reduced tumor volumes, the lung and liver metastasis potential after cells were subcutaneously injected into the hind limb of nude mice (Fig. 5J, K). In summary, these data demonstrated that MIR17HG played an oncogenic role in CRC tumorigenesis.

MIR17HG acts as a potential immunotherapeutic target in CRC by binding to PD-L1 directly

Given its importance in CRC immunity-related progression and prognosis, the potential role of MIR17HG in immunotherapy was further evaluated. As shown in Fig. 6A, the interaction of MIR17HG and several established immunotherapeutic targets, including programmed cell death ligand 1 (PD-L1), programmed cell death ligand 2 (PD-L2), T-cell immunoglobulin and mucin-domain containing-3 (TIM-3), and cytotoxic T-lymphocyte-associated antigen 4 (CTLA-4), were evaluated by RNA Pull down assay. Results showed that PD-L1 was bound with MIR17HG in both SW620 and HCT116 cells, indicating the binding between MIR17HG and PD-L1.

As reported, PD-L1 binding the PD-1 transmembrane receptor is considered to regulate T cell activation and immune responses, which achieved great success in immunotherapy (23, 24). As shown in Supplementary Fig. S7, the mRNA expression levels of PD-L1 in HCT116 and SW620 cells were indistinguishable from control,

following either MIR17HG overexpression or knockdown. However, WB assay suggested increased PD-L1 expression following MIR17HG overexpression and decreased PD-L1 expression following MIR17HG knockdown in HCT116 and SW620 cells (Fig. 6B). lncRNA could direct bind to protein and increase the stability of protein without regulation of mRNA levels (23). Therefore, we speculate that MIR17HG regulates expression of PD-L1 on the protein level, but not on the mRNA level. IHC staining suggested significantly lower expression levels of PD-L1 in tumor tissues formed by subcutaneous injection of shMIR17HG treated SW620 or HCT116 cells, compared with NC-treated control (Fig. S8 A, B). Furthermore, IHC analysis demonstrated that PD-L1 expression levels were significantly higher in tumor tissue than adjacent normal tissue in $RELA^{fl/fl}$, but not $RELA^{-/-}$ murine intestine (Fig. 6C), which exhibited the same expression trend as MIR17HG in murine tissues (shown in Fig. 2F). Additionally, correlation analysis documented that levels of PD-L1 and MIR17HG were positively correlated in CRC tissues (Fig. 6D). Moreover, CD3E, the component of the T-cell receptor–CD3 complex, is required for T-cell activation in immune therapy (24, 25). IHC staining of mice specimens showed that much more CD3E positive T cells were infiltrated from adjacent to CRC tissues in $RELA^{fl/fl}$ mice (Fig. 6E). Subsequent TMA analysis confirmed the higher expression levels of PD-L1 and CD3E in CRC than adjacent tissues (Fig. 6F). Hereby, MIR17HG might be a potential immunotherapeutic target in CRC.

Overall, our study demonstrated that the lncRNA MIR17HG promoted CRC tumorigenesis and progression by upregulating RELA in the positive feedback manner. In addition, MIR17HG, the primary precursor for miR-17-5p, suppressed the expression of its target gene BLNK. Furthermore, MIR17HG directly binds to PD-L1, thereby elevating PD-L1 levels in CRC. Hence, MIR17HG exerted pleiotropic oncogenic effects in CRC and might serve as a promising immunotherapeutic target (Fig. 6G).

Discussion

CRC is one of the most important malignancies worldwide accompanied by a high rate of morbidity and mortality (26). Although the survival of CRC patients has significantly progressed over the past decades, prognosis of patients remains poor, with 5-year overall survival rates of 10-15% (27). Additionally, recent studies have indicated that immunosuppression is involved in oncogenicity, as well as tumor development and invasion in CRC (28, 29). The present study clarified the specific mechanism of the promotion of CRC tumorigenesis and metastasis by lncRNA MIR17HG, and we propose that it may serve as a promising immunotherapeutic target.

lncRNAs are functional transcripts that regulate gene expression through diverse mechanisms. Haurte has reviewed the roles of lncRNAs in the tumorigenesis and development of cancer and indicated that post-transcriptional regulation is one of the major molecular mechanisms by which lncRNAs function in a variety of human cancers (30). In the present study, we reported the post-transcriptional regulation of MIR17HG in the tumorigenesis of CRC in two ways. Firstly, MIR17HG is the host gene for the miR-17-92 cluster, encoding a group of miRNAs (31); therefore, induces gene silencing by binding to target sites within the 3’UTR of the targeted mRNA. Secondly, MIR17HG functions as a ceRNA and bases its activity on a

sequence-specific interaction with miRNA, thus reducing their action on mRNA targets by titrating the amount of free miRNA (21).

The miR-17-92 cluster miRNAs encoded by MIR17HG are oncogenic miRNAs that have been studied in cancers (32, 33). The miR-17-92 miRNAs regulate genes involved in signaling molecules and the cell cycle (34, 35). In terms of CRC, it is reported that the miR-17-92 cluster is progressively accumulated during colorectal adenoma to adenocarcinoma progression and positively correlated to the aggressive phenotype of cancer (36). Ma *et al.* suggested that miR-17-5p promotes CRC development by targeting P130 (37). In addition, the expression level of miR-19a was significantly correlated with activated β-catenin in CRC and associated with the aggressive stage of tumor progression (38). In this study, we confirmed that the MIR17HG–miR-17-5p axis directly targeted BLNK, thus promoting the initiation and metastasis of CRC.

The tumor suppressor BLNK is a B-cell adaptor, and it plays an essential role in signal transduction by interacting with pre-B-cell and B-cell antigen receptors (39). BLNK-deficient mice show a high incidence of spontaneous pre-B-cell lymphoma due to enhanced proliferative capacity (40). Similarly, approximately 50% of human childhood pre-B acute lymphoblastic leukemia show the complete loss or a drastic reduction of BLNK expression (41). Here, we also confirmed the tumor suppressor role of BLNK in CRC.

lncRNAs can function as ceRNAs by competitively binding to miRNAs, thus positively regulating the target mRNAs (20, 21). We also determined that MIR17HG increased RELA expression without affecting miR-375 levels, indicating that MIR17HG behaves as a ceRNA. The RELA protein induces gene transcription by directly binding to the promoter region (42). In the ChIP assay, RELA directly bound to the promoter elements of MIR17HG, a positive feedback loop between MIR17HG and RELA was identified. RELA, which is constitutively activated in CRC, acts as a bridge between inflammation and cancer (43, 44). Liu *et al.* suggested that the miR-221/miR-222–RELA axis forms a positive feedback loop in CRC cells, promoting its malignant phenotypes (45). Despite the importance of RELA in CRC (46-48), it is not an ideally precise therapeutic target due to high cross-reactivity (49). Otherwise, our results suggested the targeting of MIR17HG as a potential therapeutic strategy for CRC. The lncRNA expression pattern is highly specific to tissue and cell type (50); therefore, drugs that target lncRNAs can be less toxic than conventional protein-targeting drugs (30).

Beyond these findings, we determined that MIR17HG directly bound to PD-L1 protein for accumulation in the CRC. T cell–based immunotherapy is a promising strategy for cancer treatment (51). PD-L1 is a key roadblock for T cell activation, making it an ideal target for immunotherapy (51). Therefore, our study also highlighted the potential immunotherapeutic role of MIR17HG.

In summary, this study demonstrated that MIR17HG promotes tumorigenesis and metastasis in CRC via miR-17-5p to blunt BLNK. Meanwhile, MIR17HG and RELA are involved in positive feedback regulation through a ceRNA mechanism involving miR-375 in CRC. Furthermore, MIR17HG represents a potential immunotherapeutic target by binding to PD-L1. These findings may provide new insights into the development of novel therapeutics for CRC.

Acknowledgments:

This work was financially supported by the Fund of International Cooperation and Exchange of the National Natural Science Foundation of China (81861138017), the Ministry of Foreign Affairs and International Cooperation of Italy (PGR00962), the National Natural Science Foundation of China (91643109, 81730088 and 81703261), the Natural Science Foundation of Jiangsu Province (BK20171060), the Six Talent Peaks Project in Jiangsu Province (2016-WSN-002), the Fundamental Research Funds for the Central Universities, the Postgraduate Research & Practice Innovation Program of Jiangsu Province (KYCX17_0187, KYCX18_0192).

References

1. Siegel RL, Miller KD, Jemal A. Cancer statistics, 2015. CA: a cancer journal for clinicians. 2015;65:5-29.
2. Ullman TA, Itzkowitz SH. Intestinal inflammation and cancer. Gastroenterology. 2011;140:1807-16.
3. Ruland J. Return to homeostasis: downregulation of NF-kappaB responses. Nature immunology. 2011;12:709-14.
4. Cooks T, Pateras IS, Tarcic O, Solomon H, Schetter AJ, Wilder S, et al. Mutant p53 prolongs NF-kappaB activation and promotes chronic inflammation and inflammation-associated colorectal cancer. Cancer cell. 2013;23:634-46.
5. Karin M, Greten FR. NF-kappaB: linking inflammation and immunity to cancer development and progression. Nature reviews Immunology. 2005;5:749-59.
6. Ulitsky I, Bartel DP. lincRNAs: genomics, evolution, and mechanisms. Cell. 2013;154:26-46.
7. Batista PJ, Chang HY. Long noncoding RNAs: cellular address codes in development and disease. Cell. 2013;152:1298-307.
8. Schmitt AM, Chang HY. Long Noncoding RNAs in Cancer Pathways. Cancer cell. 2016;29:452-63.
9. Kim T, Jeon YJ, Cui R, Lee JH, Peng Y, Kim SH, et al. Role of MYC-regulated long noncoding RNAs in cell cycle regulation and tumorigenesis. Journal of the National Cancer Institute. 2015;107.
10. Ma Y, Yang Y, Wang F, Moyer MP, Wei Q, Zhang P, et al. Long non-coding RNA CCAL regulates colorectal cancer progression by activating Wnt/beta-catenin signalling pathway via suppression of activator protein 2alpha. Gut. 2016;65:1494-504.
11. Esposti DD, Hernandez-Vargas H, Voegele C, Fernandez-Jimenez N, Forey N, Bancel B, et al. Identification of novel long non-coding RNAs deregulated in hepatocellular carcinoma using RNA-sequencing. Oncotarget. 2016;7:31862-77.
12. Yu X, Feng L, Liu D, Zhang L, Wu B, Jiang W, et al. Quantitative proteomics reveals the novel co-expression signatures in early brain development for prognosis of glioblastoma multiforme. Oncotarget. 2016;7:14161-71.
13. Langfelder P, Horvath S. WGCNA: an R package for weighted correlation network analysis. BMC bioinformatics. 2008;9:559.
14. Duan H, Ge W, Zhang A, Xi Y, Chen Z, Luo D, et al. Transcriptome analyses reveal molecular mechanisms underlying functional recovery after spinal cord injury. Proceedings of the National Academy of Sciences of the United States of America. 2015;112:13360-5.
15. Cioffi M, Trabulo SM, Sanchez-Ripoll Y, Miranda-Lorenzo I, Lonardo E, Dorado J, et al. The miR-17-92 cluster counteracts quiescence and chemoresistance in a distinct subpopulation of pancreatic cancer stem cells. Gut. 2015;64:1936-48.

16. Jin HY, Oda H, Lai M, Skalsky RL, Bethel K, Shepherd J, et al. MicroRNA-17~92 plays a causative role in lymphomagenesis by coordinating multiple oncogenic pathways. The EMBO journal. 2013;32:2377-91.
17. Agnelli L, Forcato M, Ferrari F, Tuana G, Todoerti K, Walker BA, et al. The reconstruction of transcriptional networks reveals critical genes with implications for clinical outcome of multiple myeloma. Clinical cancer research : an official journal of the American Association for Cancer Research. 2011;17:7402-12.
18. Fu C, Turck CW, Kurosaki T, Chan AC. BLNK: a central linker protein in B cell activation. Immunity. 1998;9:93-103.
19. Oliveira-Costa JP, de Carvalho AF, da Silveira da GG, Amaya P, Wu Y, Park KJ, et al. Gene expression patterns through oral squamous cell carcinoma development: PD-L1 expression in primary tumor and circulating tumor cells. Oncotarget. 2015;6:20902-20.
20. Cesana M, Cacchiarelli D, Legnini I, Santini T, Sthandier O, Chinappi M, et al. A Long Noncoding RNA Controls Muscle Differentiation by Functioning as a Competing Endogenous RNA. Cell. 2011;147:947.
21. Salmena L, Poliseno L, Tay Y, Kats L, Pandolfi PP. A ceRNA hypothesis: the Rosetta Stone of a hidden RNA language? Cell. 2011;146:353-8.
22. Tay Y, Rinn J, Pandolfi PP. The multilayered complexity of ceRNA crosstalk and competition. Nature. 2014;505:344-52.
23. Wang F, Yuan JH, Wang SB, Yang F, Yuan SX, Ye C, et al. Oncofetal long noncoding RNA PVT1 promotes proliferation and stem cell-like property of hepatocellular carcinoma cells by stabilizing NOP2. Hepatology. 2014;60:1278-90.
24. Couzin-Frankel J. Breakthrough of the year 2013. Cancer immunotherapy. Science. 2013;342:1432-3.
25. Powles T, Eder JP, Fine GD, Braiteh FS, Loriot Y, Cruz C, et al. MPDL3280A (anti-PD-L1) treatment leads to clinical activity in metastatic bladder cancer. Nature. 2014;515:558-62.
26. Bray F, Ferlay J, Soerjomataram I, Siegel RL, Torre LA, Jemal A. Global cancer statistics 2018: GLOBOCAN estimates of incidence and mortality worldwide for 36 cancers in 185 countries. CA: a cancer journal for clinicians. 2018;68:394-424.
27. Chand M, Keller DS, Mirnezami R, Bullock M, Bhangu A, Moran B, et al. Novel biomarkers for patient stratification in colorectal cancer: A review of definitions, emerging concepts, and data. World journal of gastrointestinal oncology. 2018;10:145-58.
28. Grady WM, Carethers JM. Genomic and epigenetic instability in colorectal cancer pathogenesis. Gastroenterology. 2008;135:1079-99.
29. Yaghoubi N, Soltani A, Ghazvini K, Hassanian SM, Hashemy SI. PD-1/ PD-L1 blockade as a novel treatment for colorectal cancer. Biomedicine & pharmacotherapy = Biomedecine & pharmacotherapie. 2019;110:312-8.
30. Huarte M. The emerging role of lncRNAs in cancer. Nature medicine. 2015;21:1253-61.

31. Kato M, Wang M, Chen Z, Bhatt K, Oh HJ, Lanting L, et al. An endoplasmic reticulum stress-regulated lncRNA hosting a microRNA megacluster induces early features of diabetic nephropathy. Nature communications. 2016;7:12864.
32. Olive V, Jiang I, He L. mir-17-92, a cluster of miRNAs in the midst of the cancer network. The international journal of biochemistry & cell biology. 2010;42:1348-54.
33. Mirzamohammadi F, Kozlova A, Papaioannou G, Paltrinieri E, Ayturk UM, Kobayashi T. Distinct molecular pathways mediate Mycn and Myc-regulated miR-17-92 microRNA action in Feingold syndrome mouse models. Nature communications. 2018;9:1352.
34. Ventura A, Young AG, Winslow MM, Lintault L, Meissner A, Erkeland SJ, et al. Targeted deletion reveals essential and overlapping functions of the miR-17 through 92 family of miRNA clusters. Cell. 2008;132:875-86.
35. Mestdagh P, Bostrom AK, Impens F, Fredlund E, Van Peer G, De Antonellis P, et al. The miR-17-92 microRNA cluster regulates multiple components of the TGF-beta pathway in neuroblastoma. Molecular cell. 2010;40:762-73.
36. Luo H, Zou J, Dong Z, Zeng Q, Wu D, Liu L. Up-regulated miR-17 promotes cell proliferation, tumour growth and cell cycle progression by targeting the RND3 tumour suppressor gene in colorectal carcinoma. The Biochemical journal. 2012;442:311-21.
37. Ma Y, Zhang P, Wang F, Zhang H, Yang Y, Shi C, et al. Elevated oncofoetal miR-17-5p expression regulates colorectal cancer progression by repressing its target gene P130. Nature communications. 2012;3:1291.
38. Li Y, Lauriola M, Kim D, Francesconi M, D'Uva G, Shibata D, et al. Adenomatous polyposis coli (APC) regulates miR17-92 cluster through beta-catenin pathway in colorectal cancer. Oncogene. 2016;35:4558-68.
39. Grabbe A, Wienands J. Human SLP-65 isoforms contribute differently to activation and apoptosis of B lymphocytes. Blood. 2006;108:3761-8.
40. Flemming A, Brummer T, Reth M, Jumaa H. The adaptor protein SLP-65 acts as a tumor suppressor that limits pre-B cell expansion. Nature immunology. 2003;4:38-43.
41. Jumaa H, Bossaller L, Portugal K, Storch B, Lotz M, Flemming A, et al. Deficiency of the adaptor SLP-65 in pre-B-cell acute lymphoblastic leukaemia. Nature. 2003;423:452-6.
42. Hayden MS, Ghosh S. Shared principles in NF-kappaB signaling. Cell. 2008;132:344-62.
43. Ben-Neriah Y, Karin M. Inflammation meets cancer, with NF-kappaB as the matchmaker. Nature immunology. 2011;12:715-23.
44. Perkins ND. The diverse and complex roles of NF-kappaB subunits in cancer. Nature reviews Cancer. 2012;12:121-32.
45. Liu S, Sun X, Wang M, Hou Y, Zhan Y, Jiang Y, et al. A microRNA 221- and 222-mediated feedback loop maintains constitutive activation of NFkappaB and STAT3 in colorectal cancer cells. Gastroenterology. 2014;147:847-59 e11.

46. Lu YX, Ju HQ, Wang F, Chen LZ, Wu QN, Sheng H, et al. Inhibition of the NF-kappaB pathway by nafamostat mesilate suppresses colorectal cancer growth and metastasis. Cancer letters. 2016;380:87-97.
47. Qin M, Zhang J, Xu C, Peng P, Tan L, Liu S, et al. Knockdown of NIK and IKKbeta-Binding Protein (NIBP) Reduces Colorectal Cancer Metastasis through Down-Regulation of the Canonical NF-kappaBeta Signaling Pathway and Suppression of MAPK Signaling Mediated through ERK and JNK. PloS one. 2017;12:e0170595.
48. Tian H, Qian J, Ai L, Li Y, Su W, Kong XM, et al. Upregulation of ASAP3 contributes to colorectal carcinogenesis and indicates poor survival outcome. Cancer science. 2017;108:1544-55.
49. Yamamoto Y, Gaynor RB. Therapeutic potential of inhibition of the NF-kappaB pathway in the treatment of inflammation and cancer. The Journal of clinical investigation. 2001;107:135-42.
50. Iyer MK, Niknafs YS, Malik R, Singhal U, Sahu A, Hosono Y, et al. The landscape of long noncoding RNAs in the human transcriptome. Nature genetics. 2015;47:199-208.
51. Wang RF, Wang HY. Immune targets and neoantigens for cancer immunotherapy and precision medicine. Cell research. 2017;27:11-37.

Table 1. Multivariate Cox regression analysis of MIR17HG expression and selected clinic pathologic variables with colorectal cancer survival

Variables	Testing cohort(n=299)		Validation cohort(n=369)		Combine cohort(n=668)	
	Adjusted HR(95%CI) [a]	P [a]	Adjusted HR(95%CI) [a]	P [a]	Adjusted HR(95%CI) [a]	P [a]
Age (＞55 VS .≤55)	1.37(1.03-1.82)	0.0286	1.68(1.27-2.24)	0.0003	1.55(1.27-1.89)	<.0001
Gender (Females VS. Males)	0.92(0.69-1.23)	0.5701	0.91(0.68-1.21)	0.4939	0.92(0.75-1.13)	0.4249
Location (Rectal VS. Colon)	0.89(0.67-1.17)	0.4022	0.83(0.63-1.09)	0.1784	0.86(0.71-1.05)	0.1370
Grade (Intermediate/High VS. low)	0.82(0.62-1.10)	0.1877	0.85(0.64-1.14)	0.2735	0.84(0.69-1.03)	0.1014
TNM (III/IV VS. I/II)	5.00(3.68-6.79)	<.0001	5.74(4.26-7.73)	<.0001	5.43(4.39-6.72)	<.0001
MIR17HG (High VS. Low)	4.99(3.43-7.27)	<.0001	8.99(6.25-12.94)	<.0001	6.34(4.92-8.16)	<.0001
BLNK (High VS. Low)	0.26(0.19-0.35)	<.0001	0.08(0.06-0.12)	<.0001	0.17(0.14-0.21)	<.0001
RELA (High VS. Low)	6.80(4.61-10.04)	<.0001	14.11(9.39-21.21)	<.0001	9.52(7.23-12.53)	<.0001
miR-17-5p (High VS. Low)	8.82(6.07-12.82)	<.0001	9.47(6.40-14.01)	<.0001	8.03(6.22-10.38)	<.0001
MIR17HG/miR-17-5p (One High VS. Both Low)	5.91(3.98-8.78)	<.0001	9.92(6.75-14.57)	<.0001	7.25(5.56-9.47)	<.0001
MIR17HG/miR-17-5p (Both High VS. Both Low)	62.62(26.34-148.86)	<.0001	28.68(17.11-48.09)	<.0001	31.69(21.06-47.70)	<.0001

[a] Adjusted for age, gender, location (Rectum or Colon), grade (Intermediate/High VS. low), and clinical stage (III/IV VS. I/II).

Figure Legends

Fig.1 Construction of the lncRNA and mRNA network involved in CRC progression by WGCNA analysis.

(A-B) A total of 6 pairs of CRC and corresponding adjacent tissues, and 6 adenoma tissue specimens were subjected to lncRNA and mRNA microarray analysis, respectively. Heatmaps revealed differentially expressed genes (6 biological replicates). (C) Cluster dendrogram of modules identified by WGCNA of lncRNA and mRNA microarray data. (D) Associations of modules with clinical characteristics. In each column group, from left to right: adjacent, ADE, and CRC groups. (E) A total of 3 modules (M1, M14, and M15) were found to be significantly correlated with CRC progression independent from gender and age (Wilcoxon test). (F) Network of immune-related mRNAs and lncRNAs in M14 and M1. (G) lncRNA–TF–mRNA network in M14, with NF-κB exhibiting the highest degree. (H) NF-κB–associated lncRNA–TF–mRNA network in M1. (I) NF-κB/RELA was predicted as a pivotal component in the co-expression network based on M1 and M14.

Fig.2 MIR17HG is accumulated in CRC and transcriptionally activated by NF-κB/RELA.

(A) The expression levels of MIR17HG and RELA in adjacent, adenoma, and CRC tissues were analyzed by qRT-PCR (n = 96 per group, $^{*}P < 0.05$, $^{***}P < 0.001$, one-way ANOVA). (B) Left panel: CRC cell lines were treated with RELA siRNA or the negative control siRNA. The expression levels of MIR17HG in the indicated cells were determined by qRT-PCR. Right panel: CRC cell lines were treated with the MIR17HG silencer or the negative control. The expression levels of RELA in the

indicated cells were determined by qRT-PCR (n = 6, $^{**}P < 0.01$, $^{***}P < 0.001$, two-tailed t-test). (C) Representative images of colons from $RELA^{fl/fl}$ and $RELA^{-/-}$ mice administered the AOM-DSS regimen (n = 10 per group, two-tailed t-test). Macroscopic images of intestines, intestine lengths, tumor counts per mouse, and tumor formation rates. (D) The overall survival of the indicated mice was assessed using the KM method. *P* values were calculated by the log-rank test (n = 20). (E-F) IHC and ISH were applied to detect RELA and MIR17HG expression, respectively, in colorectal tissues from mice with the indicated treatments. The representative images and calculated IRS are shown (n = 9, $^{*}P < 0.05$, $^{**}P < 0.01$, $^{***}P < 0.001$, compared with adjacent tissue in $RELA^{fl/fl}$ mice, Kruskal-Wallis test followed by the Dunn's multiple comparison test; $^{\#\#}P < 0.001$, compared with $RELA^{fl/fl}$ of each subgroup, two-tailed t-test). (G) Upper panel: A schematic diagram depicting the binding site of RELA in the promoter region of MIR17HG. Lower panel: The binding affinity for MIR17HG and RELA was detected by ChIP assays. (H) The levels of RELA and MIR17HG in TMA were evaluated by IHC and ISH, respectively. The representative staining images are shown. The scale bar is marked in each image. (I) KM curves depicting the overall survival of CRC patients in the combined cohort that are based upon tumoral RELA and MIR17HG levels, respectively. *P* values were calculated by the log-rank test.

Fig.3 MIR17HG promotes CRC growth and metastasis through binding with miR-17-5 to suppress BLNK.

(A) MIR17HG was predicted to repress BLNK through the miR-17-92 cluster. (B) The expression levels of miR-17-5p and BLNK in adjacent, adenoma, and CRC tissues were analyzed by qRT-PCR (n = 96 per group, $^{*}P < 0.05$, $^{***}P < 0.001$,

one-way ANOVA). (C) Schematic diagram of the construction of BLNK WT and mutant luciferase reporter plasmids. SW620 and HCT116 cells expressing BLNK WT and mutant luciferase reporter plasmids were incubated with miR-17-5p mimics and the negative control. The relative luciferase activities of the indicated cells are shown. Data are presented as the ratio of Renilla luciferase activity to Firefly luciferase activity (n = 3, $^{**}P < 0.01$, $^{***}P < 0.001$, compared with BLNK mutation and miR-NC–treated cells, ANOVA followed by Tukey's multiple comparison test). (D-E) The expression levels of BLNK in cells with the indicated treatments were determined by qRT-PCR (n = 6, $^{**}P < 0.01$, $^{***}P < 0.001$, compared with NC-treated cells within each group, two-tailed t-test). (F) Schematic diagram depicting the MIR17HG–miR-17-5p–BLNK axis. (G) Upper panel: SW620 with the indicated treatments were subjected to colony formation assay (n = 6, $^{**}P < 0.01$, compared with NC, two-tailed t-test). Lower panel: SW620 with the indicated treatments were subjected to migration and invasion assays (n = 3, $^{***}P < 0.001$, compared with NC, two-tailed t-test). (H) Upper panel: SW620 with the indicated treatments were subcutaneously injected into nude mice (n = 6). The representative images of xenografts are shown. Lower panel: Subcutaneous tumors, liver, and lung tissues of the indicated mice were harvested, and luciferase activities were analyzed (n = 6, $^{*}P < 0.05$, $^{**}P < 0.01$, compared with NC, two-tailed t-test). (I) The protein levels of BLNK in TMA were evaluated by IHC. The representative staining images are shown. (J) KM curves depicting the overall survival of CRC patients in the combined cohort, based upon tumoral BLNK levels. *P* values were calculated by the log-rank test.

Fig.4 The molecular pathway RELA/MIR17HG/miR-17-5p/BLNK is involved in CRC tumorigenesis.

(A-B) ISH and IHC were applied to detect miR-17-5p and BLNK expression, respectively, in colorectal tissues from the indicated mice. The representative images and calculated scores are shown (n = 9, $^{*}P < 0.05$, $^{***}P < 0.001$, compared with adjacent tissue in $RELA^{fl/fl}$ mice, Kruskal-Wallis test followed by the Dunn's multiple comparison test; $^{\#\#\#}P < 0.001$, compared with $RELA^{fl/fl}$ of each subgroup, two-tailed t-test). The scale bar is marked in each image. (C-E) The expression levels of BLNK in cells with the indicated treatments were determined by qRT-PCR (n = 6, $^{***}P < 0.001$, compared with NC-treated cells within each group, two-tailed t-test). (F) Schematic diagram depicting the RELA–MIR17HG–miR-17-5p–BLNK axis.

Fig.5 MIR17HG plays an oncogenic role in CRC tumorigenesis through the positive feedback loop of MIR17HG/RELA by sponging miR-375.

(A) Bioinformatics analysis suggested that MIR17HG might be a ceRNA that is sponging miRNAs. (B) RIP qRT-PCR detection of the indicated RNAs retrieved by GFP antibodies in SW620 with the indicated treatments (n = 3, $^{**}P < 0.01$, compared with GFP transfected cells within each group, ANOVA followed by the Tukey's multiple comparison test). (C) The expression levels of miR-375 in adjacent, adenoma, and CRC tissues were determined by qRT-PCR (n = 96 per group, one-way ANOVA). (D) Luciferase activities in cells with the indicated treatments (n = 3, $^{***}P < 0.001$, ANOVA followed by the Tukey's multiple comparison test). (E) The expression levels of RELA in the indicated cells were determined by qRT-PCR (n = 6, $^{***}P < 0.001$, compared with NC-treated cells within each group, two-tailed t-test). (F) The expression levels of RELA in the indicated cells were determined by qRT-PCR (n = 6, $^{**}P < 0.01$, $^{***}P < 0.001$, compared with NC-treated cells within each group; $^{\#\#\#}P <$

0.001, co-overexpression compared with MIR17HG OEX / miR-375 NC within each group, two-tailed *t*-test). (G) A Schematic diagram of the MIR17HG-involved ceRNA network. (H-I) SW620 and HCT116 cells with the indicated treatments were subjected to colony formation assay (n = 6, $^{***}P < 0.001$, compared with NC, two-tailed t-test) as well as migration and invasion assays (n = 3, $^{***}P < 0.001$, compared with NC, two-tailed t-test). (J-K) SW620 and HCT116 cells with the indicated treatments were subcutaneously injected into nude mice. The representative images of xenografts are shown. Subcutaneous tumors, liver and lung tissues of the indicated mice were harvested, and luciferase activities were analyzed (n = 6, $^{*}P < 0.05$, $^{**}P < 0.01$, compared with NC, two-tailed t-test).

Fig.6 MIR17HG binds directly to PD-L1, making it a potential immunotherapeutic target for CRC.

(A) RNA pull down assay suggested binding of MIR17HG to PD-L1. (B) Western blot was employed to detect the protein levels of PD-L1 in the indicated cells. (C) IHC was applied to detect PD-L1 expression in murine tissues with the indicated treatments. The representative images and calculated IRS are shown (n = 9, $^{***}P < 0.001$, compared with adjacent tissue in $RELA^{fl/fl}$ mice; $^{\#\#}P < 0.01$, $^{\#\#\#}P < 0.001$, compared with $RELA^{fl/fl}$ of each subgroup, two-tailed t-test). (D) Correlation between MIR17HG and PD-L1 expression levels in CRC tissues (n = 96, Fisher r-to-z transformation test followed by the Pearson correlation test). (E) The levels of CD3E in murine tissues were evaluated by IHC analysis, and the representative staining images and the calculated IRS are shown (n = 9, $^{***}P < 0.001$, compared with adjacent tissues from $RELA^{fl/fl}$ mice; $^{\#\#\#}P < 0.001$, compared with $RELA^{fl/fl}$ of each subgroup, two-tailed t-test). (F) The levels of PD-L1 and CD3E in TMA were evaluated by IHC,

and the staining score differences between CRC lesions and adjacent tissues (cancer - adjacent) are shown. The scale bar is marked in each image. (G) The systemic molecular pathway of MIR17HG-mediated tumorigenesis.

Figure 1

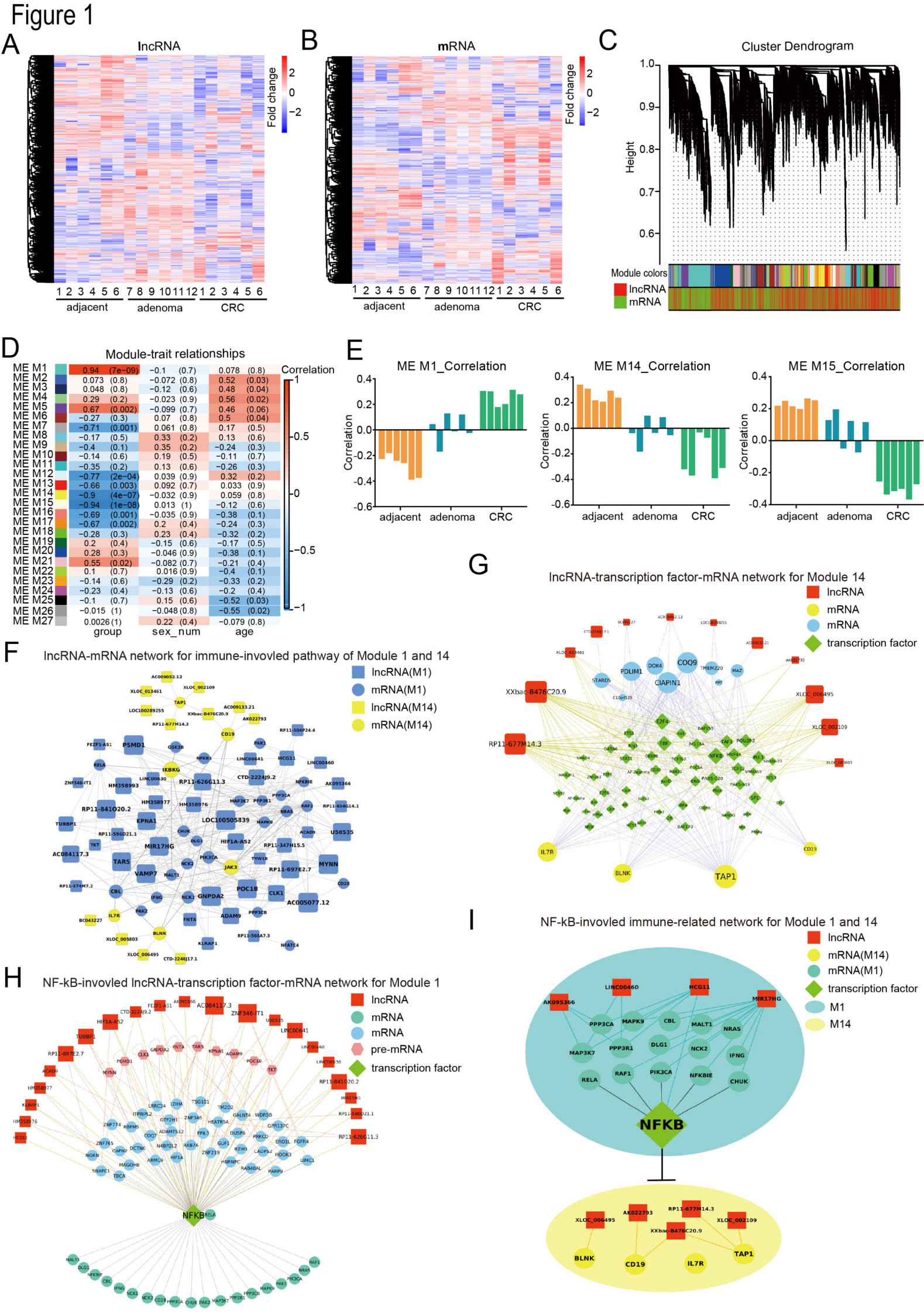
A
lncRNA
Fold change
2
0
−2
1 2 3 4 5 6 7 8 9 10 11 12 1 2 3 4 5 6
adjacent
adenoma
CRC
B
mRNA
Fold change
2
0
−2
1 2 3 4 5 6 7 8 9 10 11 12 1 2 3 4 5 6
adjacent
adenoma
CRC
C
Cluster Dendrogram
Height
1.0
0.9
0.8
0.7
0.6
Module colors
lncRNA
mRNA
D
Module-trait relationships
ME M1 0.94 (7e−09) −0.1 (0.7) 0.078 (0.8)
ME M2 0.073 (0.8) −0.072 (0.8) 0.52 (0.03)
ME M3 0.048 (0.8) −0.12 (0.6) 0.48 (0.04)
ME M4 0.29 (0.2) −0.023 (0.9) 0.56 (0.02)
ME M5 0.67 (0.002) −0.099 (0.7) 0.46 (0.06)
ME M6 −0.27 (0.3) 0.07 (0.8) 0.5 (0.04)
ME M7 −0.71 (0.001) 0.061 (0.8) 0.17 (0.5)
ME M8 −0.17 (0.5) 0.33 (0.2) 0.13 (0.6)
ME M9 −0.4 (0.1) 0.35 (0.2) −0.24 (0.3)
ME M10 −0.14 (0.6) 0.19 (0.5) −0.11 (0.7)
ME M11 −0.35 (0.2) 0.13 (0.6) −0.26 (0.3)
ME M12 −0.77 (2e−04) 0.039 (0.9) 0.32 (0.2)
ME M13 −0.66 (0.003) 0.092 (0.7) 0.033 (0.9)
ME M14 −0.9 (4e−07) −0.032 (0.9) 0.059 (0.8)
ME M15 −0.94 (1e−08) 0.013 (1) −0.12 (0.6)
ME M16 −0.69 (0.001) −0.035 (0.9) −0.38 (0.1)
ME M17 −0.67 (0.002) 0.2 (0.4) −0.24 (0.3)
ME M18 −0.28 (0.3) 0.23 (0.4) −0.32 (0.2)
ME M19 0.2 (0.4) −0.15 (0.6) −0.17 (0.5)
ME M20 0.28 (0.3) −0.046 (0.9) −0.38 (0.1)
ME M21 0.55 (0.02) −0.082 (0.7) −0.21 (0.4)
ME M22 0.1 (0.7) 0.016 (0.9) −0.4 (0.1)
ME M23 −0.14 (0.6) −0.29 (0.2) −0.33 (0.2)
ME M24 −0.23 (0.4) −0.13 (0.6) −0.2 (0.4)
ME M25 −0.1 (0.7) 0.15 (0.6) −0.52 (0.03)
ME M26 −0.015 (1) −0.048 (0.8) −0.55 (0.02)
ME M27 0.0026 (1) 0.22 (0.4) −0.079 (0.8)
group
sex_num
age
Correlation
1
0.5
0
−0.5
−1
E
ME M1_Correlation
ME M14_Correlation
ME M15_Correlation
Correlation
adjacent
adenoma
CRC
F
lncRNA-mRNA network for immune-invovled pathway of Module 1 and 14
lncRNA(M1)
mRNA(M1)
lncRNA(M14)
mRNA(M14)
G
lncRNA-transcription factor-mRNA network for Module 14
lncRNA
mRNA
mRNA
transcription factor
XXbac-B476C20.9
RP11-677M14.3
XLOC_006495
XLOC_002109
IL7R
BLNK
TAP1
CD19
H
NF-kB-invovled lncRNA-transcription factor-mRNA network for Module 1
lncRNA
mRNA
mRNA
pre-mRNA
transcription factor
NFKB
I
NF-kB-invovled immune-related network for Module 1 and 14
lncRNA
mRNA(M14)
mRNA(M1)
transcription factor
M1
M14
NFKB
XLOC_006495
AK022793
RP11-677M14.3
XXbac-B476C20.9
XLOC_002109
BLNK
CD19
IL7R
TAP1

Figure 2

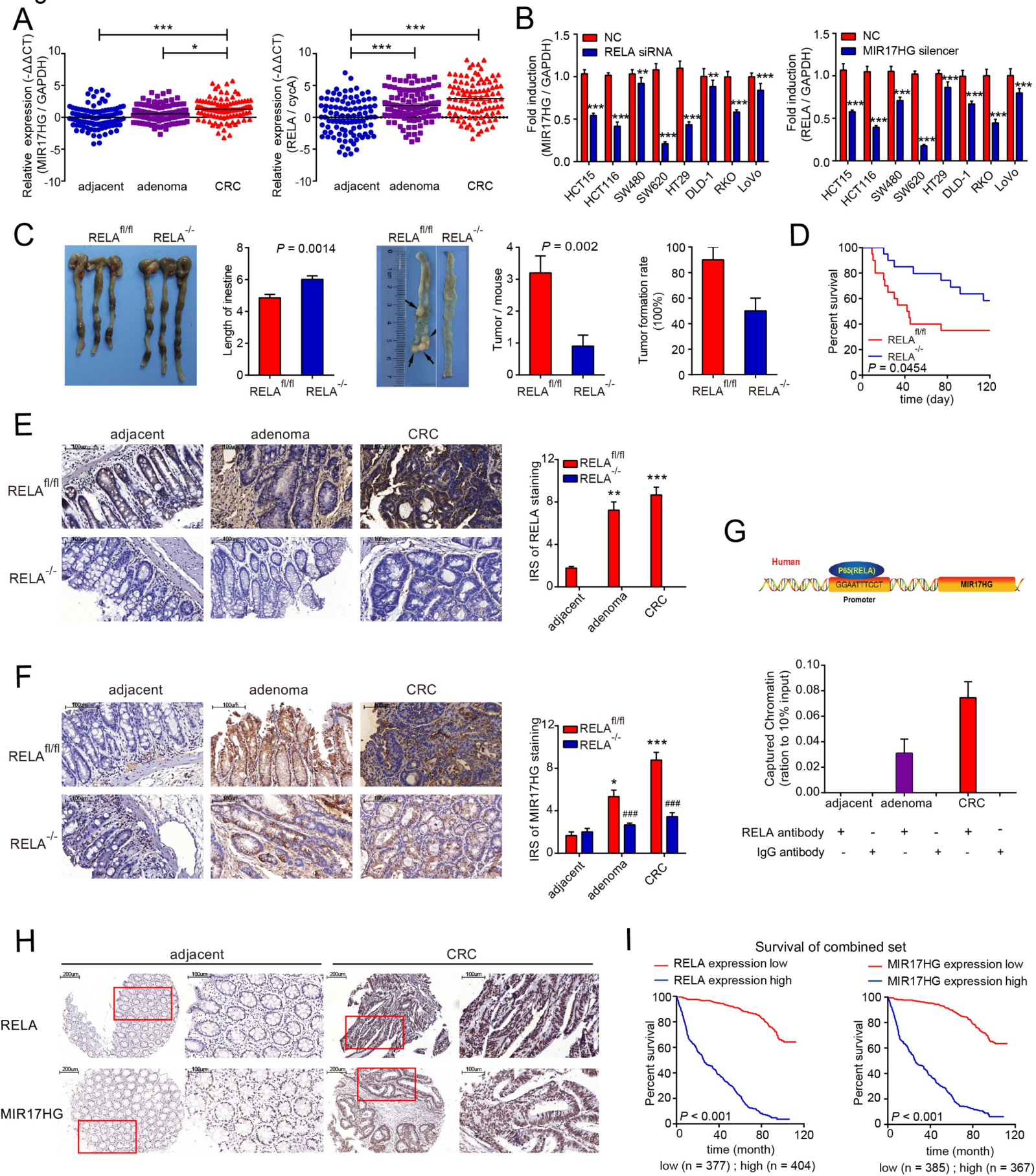
A
Relative expression (-ΔΔCT) (MIR17HG / GAPDH)
adjacent
adenoma
CRC
Relative expression (-ΔΔCT) (RELA / cycA)
B
NC
RELA siRNA
Fold induction (MIR17HG / GAPDH)
MIR17HG silencer
Fold induction (RELA / GAPDH)
HCT15
HCT116
SW480
SW620
HT29
DLD-1
RKO
LoVo
C
RELA fl/fl
RELA -/-
P = 0.0014
Length of inestine
P = 0.002
Tumor / mouse
Tumor formation rate (100%)
D
Percent survival
P = 0.0454
time (day)
E
adjacent
adenoma
CRC
IRS of RELA staining
F
IRS of MIR17HG staining
Captured Chromatin (ration to 10% input)
RELA antibody
IgG antibody
G
Human
P65(RELA)
GGAATTTCCT
MIR17HG
Promoter
H
RELA
MIR17HG
I
Survival of combined set
RELA expression low
RELA expression high
MIR17HG expression low
MIR17HG expression high
P < 0.001
time (month)
low (n = 377) ; high (n = 404)
low (n = 385) ; high (n = 367)

Figure 3

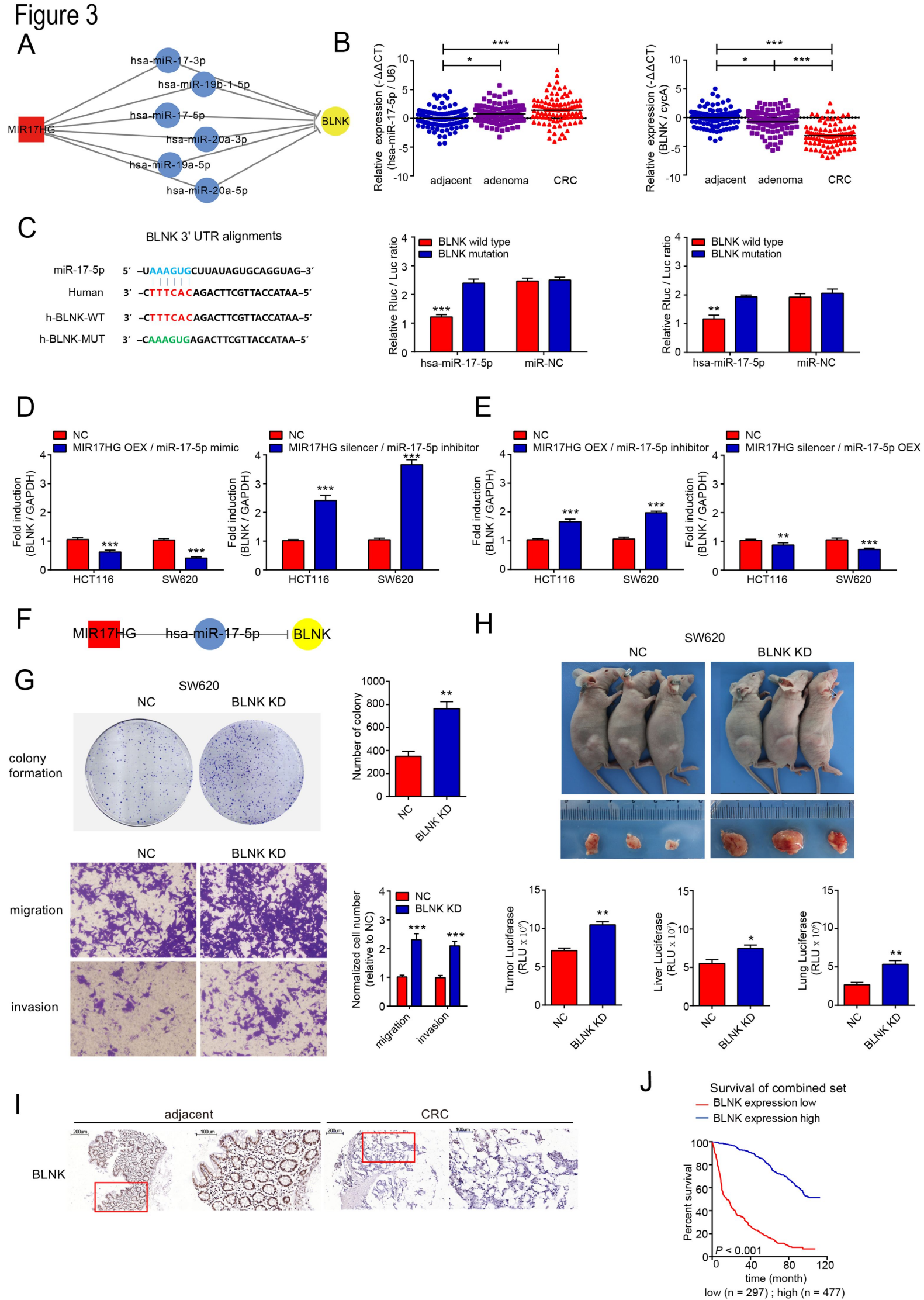
A
hsa-miR-17-3p
hsa-miR-19b-1-5p
hsa-miR-17-5p
hsa-miR-20a-3p
hsa-miR-19a-5p
hsa-miR-20a-5p
MIR17HG
BLNK
B
Relative expression (-ΔΔCT) (hsa-miR-17-5p / U6)
adjacent
adenoma
CRC
Relative expression (-ΔΔCT) (BLNK / cycA)
C
BLNK 3' UTR alignments
miR-17-5p 5′ –UAAAGUGCUUAUAGUGCAGGUAG–3′
Human 3′ –CTTTCACAGACTTCGTTACCATAA–5′
h-BLNK-WT 3′ –CTTTCACAGACTTCGTTACCATAA–5′
h-BLNK-MUT 3′ –CAAAGUGAGACTTCGTTACCATAA–5′
BLNK wild type
BLNK mutation
Relative Rluc / Luc ratio
hsa-miR-17-5p
miR-NC
D
NC
MIR17HG OEX / miR-17-5p mimic
MIR17HG silencer / miR-17-5p inhibitor
Fold induction (BLNK / GAPDH)
HCT116
SW620
E
MIR17HG OEX / miR-17-5p inhibitor
MIR17HG silencer / miR-17-5p OEX
F
MIR17HG
hsa-miR-17-5p
BLNK
G
SW620
NC
BLNK KD
colony formation
Number of colony
migration
invasion
Normalized cell number (relative to NC)
H
Tumor Luciferase (RLU x 10⁹)
Liver Luciferase (RLU x 10⁷)
Lung Luciferase (RLU x 10⁶)
I
adjacent
CRC
BLNK
J
Survival of combined set
BLNK expression low
BLNK expression high
Percent survival
P < 0.001
time (month)
low (n = 297) ; high (n = 477)

Figure 4

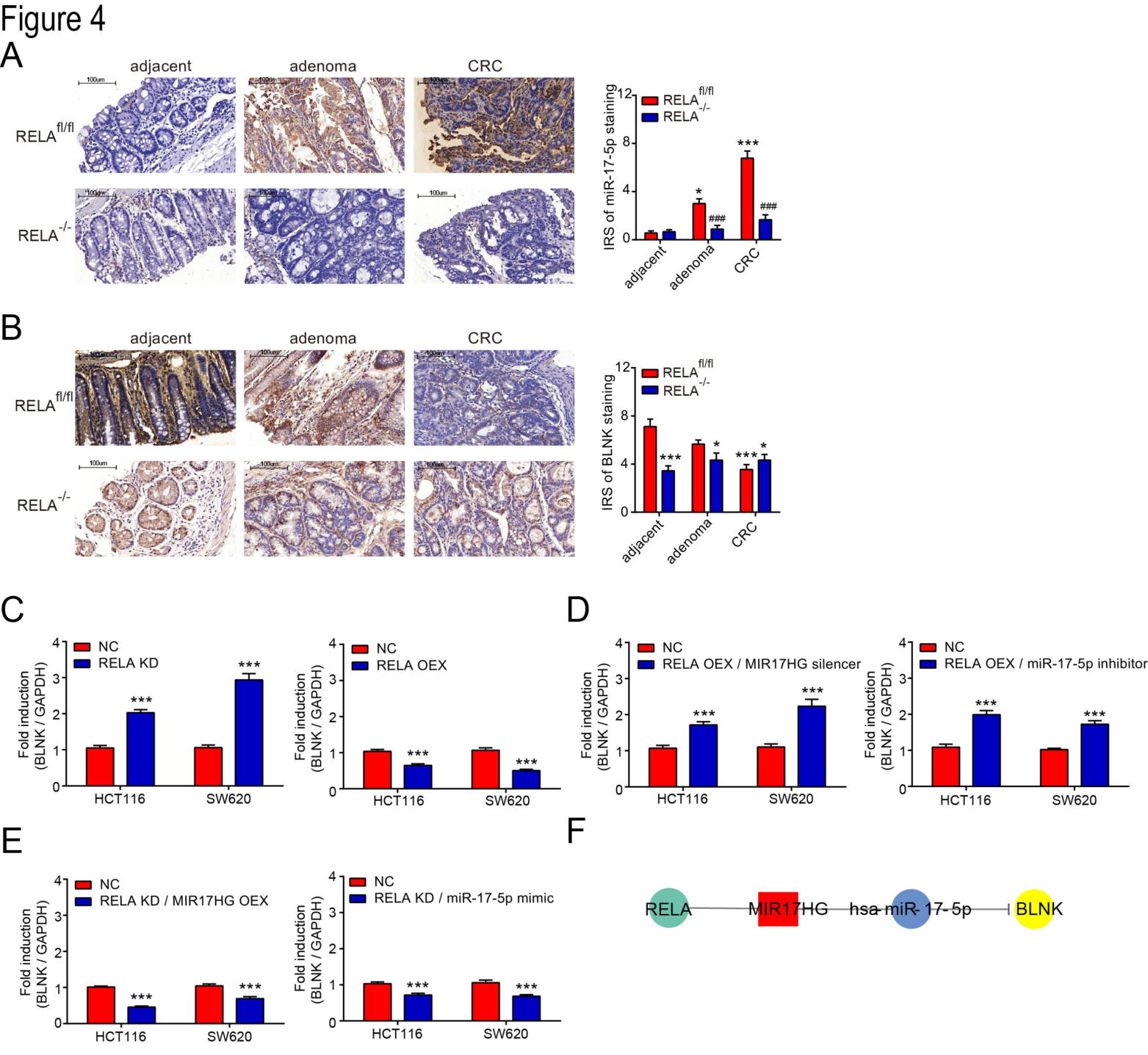
A
adjacent
adenoma
CRC
RELA fl/fl
RELA -/-
IRS of miR-17-5p staining
B
IRS of BLNK staining
C
NC
RELA KD
RELA OEX
Fold induction (BLNK / GAPDH)
HCT116
SW620
D
RELA OEX / MIR17HG silencer
RELA OEX / miR-17-5p inhibitor
E
RELA KD / MIR17HG OEX
RELA KD / miR-17-5p mimic
F
RELA
MIR17HG
hsa-miR-17-5p
BLNK

Figure 5

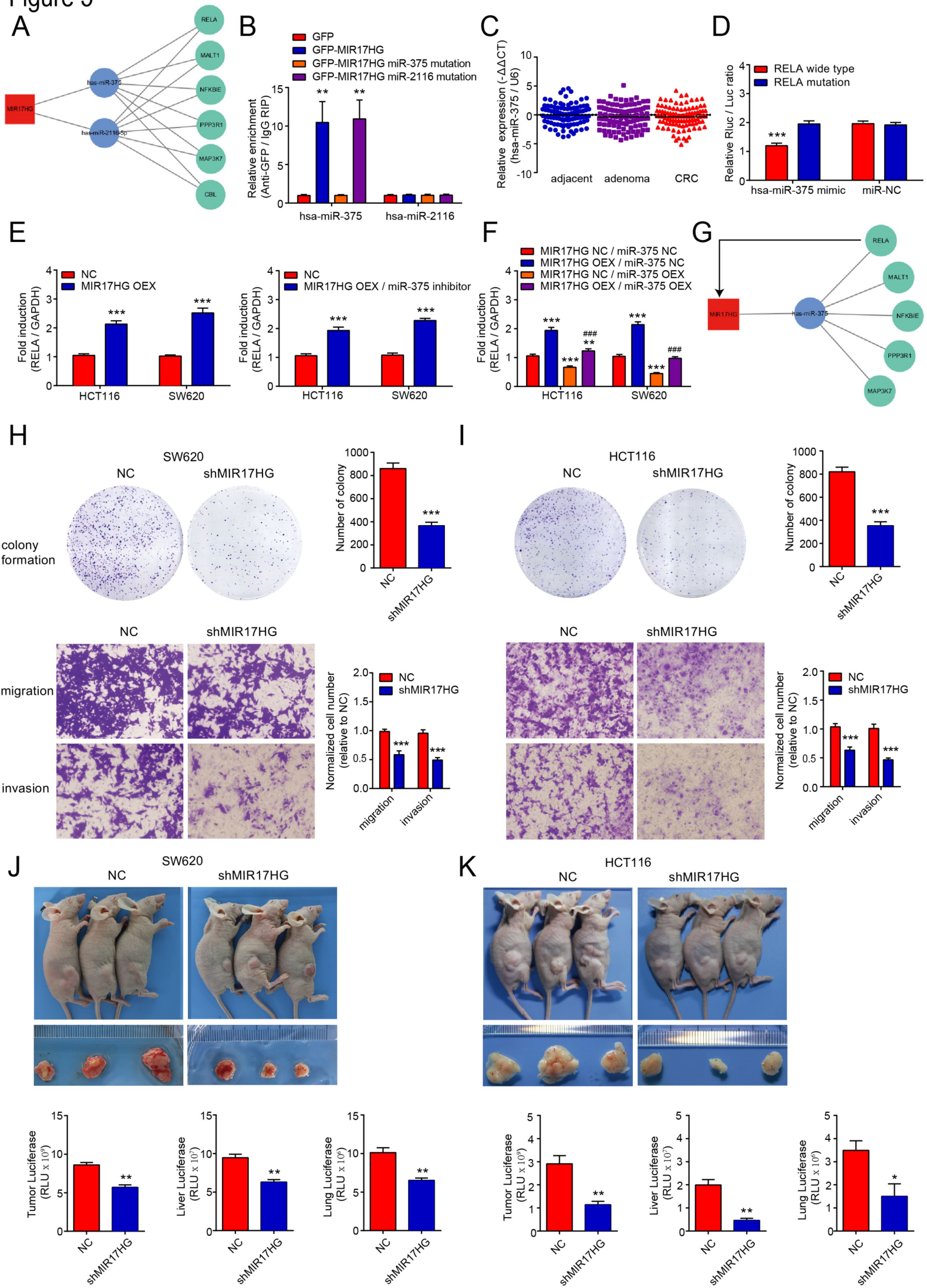
A
RELA
MALT1
NFKBIE
PPP3R1
MAP3K7
CBL
has-miR-375
has-miR-2116-5p
MIR17HG
B
GFP
GFP-MIR17HG
GFP-MIR17HG miR-375 mutation
GFP-MIR17HG miR-2116 mutation
Relative enrichment (Anti-GFP / IgG RIP)
hsa-miR-375
hsa-miR-2116
C
Relative expression (-ΔΔCT) (hsa-miR-375 / U6)
adjacent
adenoma
CRC
D
RELA wide type
RELA mutation
Relative Rluc / Luc ratio
hsa-miR-375 mimic
miR-NC
E
NC
MIR17HG OEX
Fold induction (RELA / GAPDH)
HCT116
SW620
MIR17HG OEX / miR-375 inhibitor
F
MIR17HG NC / miR-375 NC
MIR17HG OEX / miR-375 NC
MIR17HG NC / miR-375 OEX
MIR17HG OEX / miR-375 OEX
G
H
SW620
NC
shMIR17HG
colony formation
Number of colony
migration
invasion
Normalized cell number (relative to NC)
I
HCT116
J
SW620
K
HCT116
Tumor Luciferase (RLU x 10⁹)
Liver Luciferase (RLU x 10⁷)
Lung Luciferase (RLU x 10⁶)

Figure 6

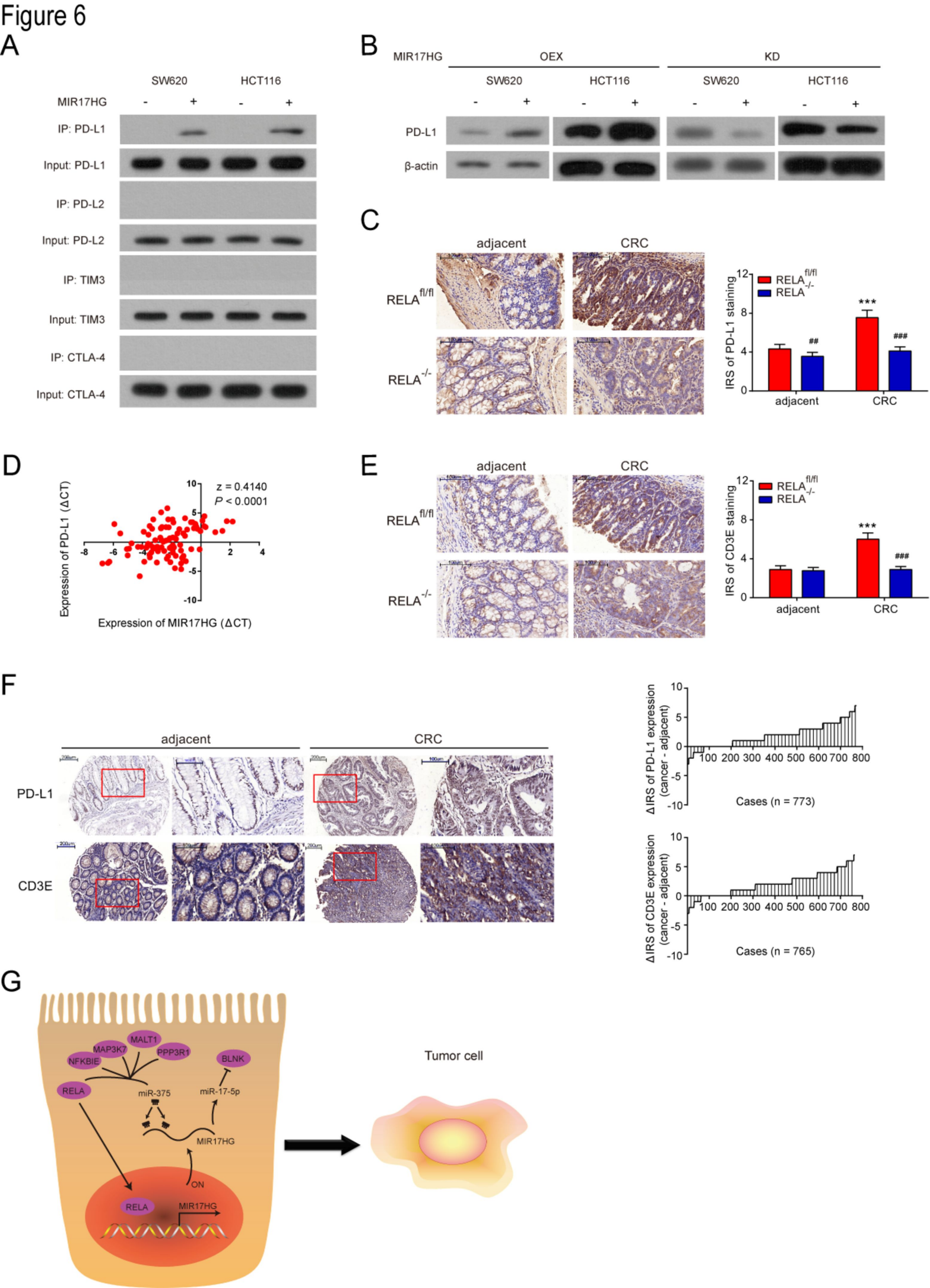
A
SW620
HCT116
MIR17HG
IP: PD-L1
Input: PD-L1
IP: PD-L2
Input: PD-L2
IP: TIM3
Input: TIM3
IP: CTLA-4
Input: CTLA-4
B
MIR17HG
OEX
KD
SW620
HCT116
PD-L1
β-actin
C
adjacent
CRC
RELA fl/fl
RELA -/-
IRS of PD-L1 staining
adjacent
CRC
D
z = 0.4140
P < 0.0001
Expression of PD-L1 (ΔCT)
Expression of MIR17HG (ΔCT)
E
IRS of CD3E staining
F
PD-L1
CD3E
ΔIRS of PD-L1 expression (cancer - adjacent)
Cases (n = 773)
ΔIRS of CD3E expression (cancer - adjacent)
Cases (n = 765)
G
MALT1
MAP3K7
PPP3R1
NFKBIE
BLNK
RELA
miR-375
miR-17-5p
MIR17HG
ON
Tumor cell